Int. J. Multiphase Flow Vol. 18, No. 6, pp. 877–890, 1992
Printed in Great Britain.

0301-9322/92 $5.00 + 0.00

MEASUREMENT OF HEAT TRANSFER AT THE PHASE INTERFACE OF CONDENSING BUBBLES

Y. M. CHEN[1] and F. MAYINGER[2]

[1]Department of Mechanical Engineering, National Taiwan University, Taipei, Taiwan

[2]Lehrstuhl A für Thermodynamik, Technische Universität München, München, Germany

(Received 15 November 1990; in revised form 30 July 1992)

Abstract—Using holographic interferometry and high-speed cinematography the heat transfer at the phase interface of vapor bubbles condensing in a subcooled liquid of the same substance was measured with ethanol, propanol, refrigerant R113 and water. To evaluate the axisymmetric temperature field around the bubble from the interference fringe field, the Abel integral method is not sufficient. A correction procedure considering the light deflection caused by the local temperature gradient has been developed and applied to calculate the heat transfer coefficient. The measurements were performed in the range $2 < \mathrm{Pr} < 15$ and $1 < \mathrm{Ja} < 120$. Measured data could be well-correlated as functions of the Prandtl and Reynolds numbers for the heat transfer coefficient and as functions of the Reynolds, Prandtl and Jacob numbers for the bubble collapse time.

Key Words: bubble condensation, holographic interferometry

1. INTRODUCTION

The thermo- and hydrodynamic phenomena during the collapse of vapor bubbles in liquids having a temperature below saturation conditions—so-called subcooled liquids—are of technical and scientific interest for a better understanding of the instability condition in two-phase flow with subcooled boiling and in cavitation. The temporal course of the collapse of a vapor bubble during condensation in a subcooled liquid can be controlled by two different phenomena: (1) the heat transfer at the phase interface of the vapor and liquid; and (2) the inertia of the liquid mass when entering into the space created by the condensing vapor.

With moderate temperature differences between the vapor and subcooled liquid the heat transport will be the governing process for the volumetric decrease of the bubble. This heat transfer process at the phase interface is influenced by the thermophysical properties, like heat conductivity, specific heat, latent heat of vaporization, density and viscosity. Also, the gradient of the saturation curve plays a role. The thermophysical properties can be expressed in dimensionless numbers like the Prandtl ($\mathrm{Pr} = \eta_L c_p/\lambda_L$; η_L is liquid viscosity, λ_L is liquid thermal conductivity) and Jacob [$\mathrm{Ja} = \rho_L c_p(T_s - T_\infty)/\rho_G \Delta h$; ρ_L and ρ_G are the gas and liquid density, T_s is the saturation temperature and h is the heat transfer coefficient] numbers. With bubbles moving in the liquid, the Reynolds number [$\mathrm{Re} = \rho_L W(2R)/\eta_L$; W is velocity and R is bubble radius] has to be taken into account. Also the Fourier number ($\mathrm{Fo} = a_L t/2R$; a_L is thermal diffusivity of the liquid and t is time) can be used as a dimensionless time to describe the duration of the collapsing period.

There is a large number of theoretical and experimental studies in the literature dealing with the condensation of bubbles. An extensive and comprehensive discussion of the state of the art can be found, for example, in the papers by Hammitt (1980) and Theofanous *et al.* (1970). In the case of inertia-controlled condensation, Plesset & Prosperetti (1979) and Hammitt & Kling (1972) found good agreement with Rayleigh's (1917) correlation. The situation with heat-transport-controlled condensation seems to be more complicated. Various authors describe the heat transfer at the phase interface of a condensing bubble as similar to that around a moving solid sphere (Moalem & Sideman 1973; Akiyama 1973) or a liquid droplet (Voloshko *et al.* 1973). Examples of equations describing the bubble collapse (Floschuetz & Chao 1965; Voloshko & Vurgaft 1971; Dimic 1977) are presented in table 1. The agreement of data predicted with these equations is not too good, which may be mainly due to the unknown heat transfer conditions. Therefore, in the present study, holographic interferometry was used to gain better insight into the thermal and fluid dynamic behavior at the phase interface and thereby attain information on the heat transfer conditions.

2. EXPERIMENTAL TECHNIQUE

In the literature the following techniques are reported for generating bubbles in a subcooled liquid: (1) superheating of a liquid boundary on a heated surface; (2) blowing saturated vapor through a nozzle into subcooled liquid; (3) flashing by depressurization; and (4) local heating by a focused laser beam. To guarantee that the boundary conditions were as simple and as homogeneous as possible in the experiments, the bubbles were produced by blowing saturated vapor through a nozzle, shown in figure 1, into a subcooled liquid moving slowly downwards.

The vapor needed for generating the bubbles flows through the channel in the center to the small chamber situated at the inner end of the nozzle. The nozzle consists of a short capillary of dia = 1.6 mm. Around this central channel vapor is flowing in an annulus acting as guardheater, guaranteeing that the vapor for generating the bubbles is saturated. Before starting the bubble formation the capillary is closed at its inner end by a needle to prevent liquid entering the nozzle.

The liquid in which the bubble is forming and collapsing was degassed extremely carefully and then cooled to a temperature temporally and locally as constant as possible. The latent heat of vaporization of the condensing vapor in the bubble raises the temperature of the liquid. Therefore, to guarantee that each bubble finds the same and equally subcooled temperature field the liquid flows with a velocity approx. 2 cm/s downwards against the nozzle. This small velocity does not have much influence on the detachment and rising velocity of the bubble.

As mentioned above, the heat transfer at the phase interface was investigated by holographic interferometry in combination with high-speed cinematography. The optical setup is shown schematically in figure 2. An argon-ion laser is used as the light source. To obtain a short exposure time for each frame, the argon laser is externally modulated by an acousto-optic modulator. The laser pulses are triggered synchronously with the rotation of the prism in the high-speed camera. To perform measurements on bubbles, the real-time method was used.

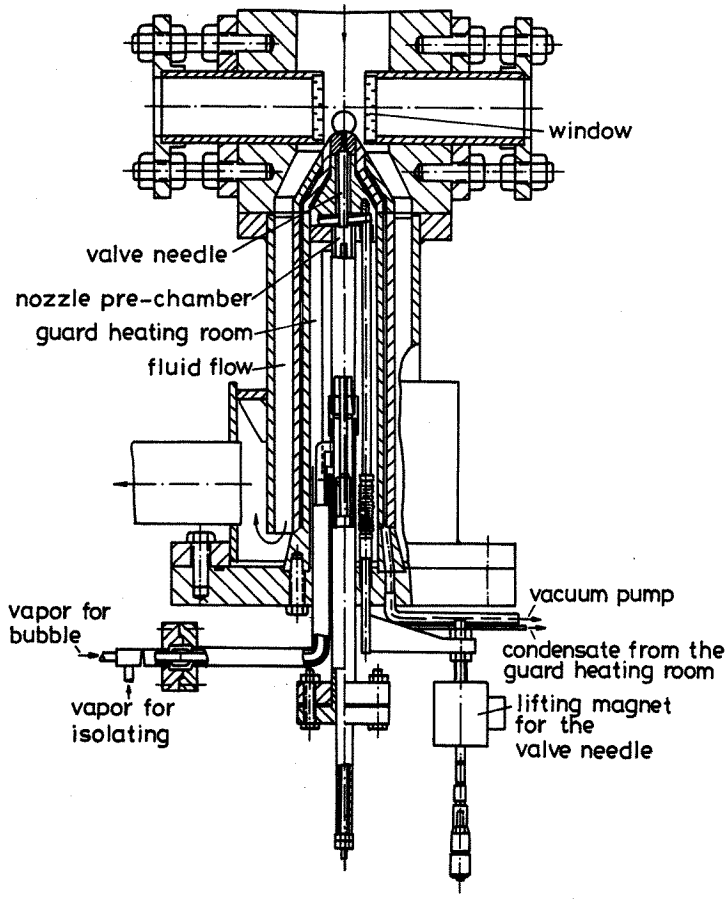

Figure 1. Test section.

3. INTERFEROGRAM ANALYSIS

To analyze the interferogram, the method known in the literature—e.g. the Abel integral (Hauf & Grigull 1970)—is not sufficient. Here one must take into account that the beam which passes through the temperature field around the bubble suffers a non-negligible deflection, caused by the large local temperature gradient. Therefore, the following correction procedure has been developed.

In this study the field of the refractive index (n) is described by a polynomial function as

$$n(r) = n_\infty + \sum_{k=1}^{k} a_k (R - r)^{k+1}, \quad r_B \leqslant r \leqslant R, \tag{1}$$

where r is the radial coordinate, k is the degree of the polynomial and $n(R) = n_\infty, \dot{n}(R) = 0$. In the above equation, r_B is the actual bubble radius and R is the radius measured optically from the bubble center to the edge of the thermal boundary layer. Initially, an analysis of the interferogram is performed ignoring the deflection of the light beam:

$$\varepsilon(y)\lambda_0 = \int_{-z_0}^{+z_0} [n(r) - n_\infty]\,dz, \quad r_B \leqslant y. \tag{2}$$

With the above equation the phase shift between the measured and the reference wave is calculated by means of the order of fringes $\varepsilon(y)$ and the wavelength λ_0 of the incident light. B inserting [1] into [2] we obtain

$$\varepsilon(y) = \frac{2}{\lambda_0} \int_0^{z_0} \left[\sum_{k=1}^{K} a_k (R - r)^{k+1} \right] dz \tag{3}$$

and after rearranging and introducing the parameter $c_k(y)$,

$$c_k(y) = \frac{2}{\lambda_0} \sum_{i=0}^{k+1} \binom{k+1}{i} (-1)^i R^{k+1-i} \int_0^{z_0} r^i\,dz$$

where

$$z_0 = \sqrt{R^2 - y^2}, \qquad r = \sqrt{y^2 + z^2}, \tag{4}$$

the equation

$$\varepsilon(y) = \frac{2}{\lambda_0} \sum_{k=1}^{K} a_k c_k(y) \tag{5}$$

can be deduced. The factors a_k can be evaluated numerically with the least squares method:

$$\phi = \sum_{n=1}^{N} [\varepsilon_n - \varepsilon(y_n)]^2 = \sum_{n=1}^{N} \left[\varepsilon_n - \sum_{k=1}^{K} a_k c_k(y_n) \right]^2, \tag{6}$$

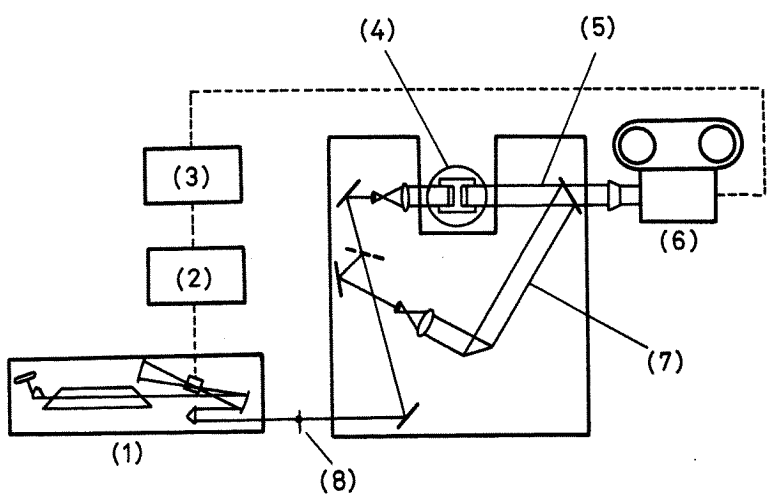

Figure 2. Optical setup of the holographic interferometer: (1) argon laser, (2) Bragg cell, (3) pulse unit, (4) test section, (5) object wave, (6) high-speed camera, (7) reference wave, (8) shutter.

where ε_n is the measured order of fringes and N is the number of interference fringes. The mathematical condition for a minimum of ϕ reads as follows:

$$\frac{\partial \phi}{\partial a_j} = -2 \sum_{n=1}^{N} \left[\varepsilon_n - \sum_{k=1}^{K} a_k c_k(y_n) \right] c_j(y_n), \quad j = 1 \text{ to } K, \tag{7}$$

or

$$\sum_{k=1}^{K} a_k \sum_{n=1}^{N} c_j(y_n) c_k(y_n) = \sum_{n=1}^{N} \varepsilon_n c_j(y_n). \tag{8}$$

The above equation can be transformed into matrix notation:

$$(E)_{jk} = \sum_{n=1}^{N} c_j(y_n) c_k(y_n), \tag{9}$$

$$(b)_i = \sum_{n=1}^{N} \varepsilon_n c_j(y_n), \tag{10}$$

where

$$E \cdot a = b, \qquad a = E^{-1} \cdot b, \tag{11}$$

from which the coefficient a of the refractive index polynomial can be evaluated.

When considering the light beam deflection, the analysis of the interferogram is much more complicated than that discussed above. Figure 3 shows an example of the deflection of a beam which runs through the liquid boundary layer in the middle section of a bubble. Due to the continuously changing temperature in the boundary and the resulting change of the refractive index, this beam has a curved trajectory. For an observer beyond the image plane it seems to come from the projected point F on the focusing plane. In the image plane the object beam interferes with the reference beam which was not deflected. Both beams have the same phase relationship up to points A and D. Assuming we have ideal lenses, the optical path length of the two beams behind the points B and C to the image plane is equal. Therefore, the interference only originates from the optical phase shift difference of the object beam running through the liquid thermal boundary layer:

$$\varepsilon(y)\lambda_0 = \int_A^B n \, ds - n_\infty \overline{DC}. \tag{12}$$

The path of the beam in the boundary layer is described by the following differential equation:

$$\ddot{y} = \frac{1}{n}(1 + \dot{y}^2)\left(\frac{\partial n}{\partial y} - \dot{y} \frac{\partial n}{\partial z} \right), \tag{13}$$

where dots refer to the differentiation with respect to z. From [12] and [13] a new distribution of the interference fringes $\varepsilon(y)$ can then be evaluated numerically. This distribution can be approached

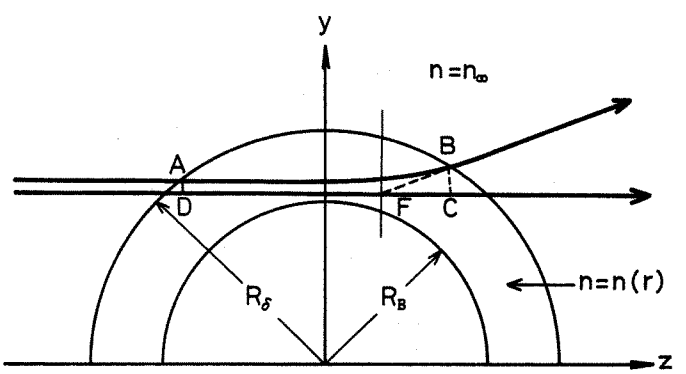

Figure 3. Formation of an interferogram.

by a correction of the polynomial coefficients a_k, which are evaluated ignoring the light deflection, with the least squares method:

$$\varepsilon(y) = \varepsilon(y, a_k) = \varepsilon(y, a_k^0 + \Delta a_k)$$

$$= \varepsilon(y, a_k) + \sum_{k=1}^{K} \left(\frac{\partial \varepsilon}{\partial a_k}\right)_{a_k = a_k^0} \Delta a_k, \qquad [14]$$

$$\phi = \sum_{n=1}^{N} [\varepsilon_n - \varepsilon(y_n, a_k)]^2$$

$$= \sum_{n=1}^{N} \left[\varepsilon_n - \varepsilon(y_n, a_k^0) - \sum_{k=1}^{K} \left(\frac{\partial \varepsilon}{\partial a_k}\right)_{a_k = a_k^0} \Delta a_k\right]^2 \qquad [15]$$

and

$$\frac{\partial \phi}{\partial \Delta a_j} = -2 \sum_{n=1}^{N} \left[\varepsilon_n - \varepsilon(y_n, a_k^0) - \sum_{k=1}^{K} \left(\frac{\partial \varepsilon}{\partial a_k}\right)_{a_k = a_k^0} \Delta a_k\right] \left(\frac{\partial \varepsilon}{\partial a_j}\right)_{a_j = a_j^0} = 0. \qquad [16]$$

Changing the above equations to matrix notation with

$$(A)_{jk} = \sum_{n=1}^{N} \left(\frac{\partial \varepsilon}{\partial a_j}\right)_{a_j = a_j^0} \left(\frac{\partial \varepsilon}{\partial a_k}\right)_{a_k = a_k^0} \qquad [17]$$

and

$$(U)_j = \sum_{n=1}^{N} [\varepsilon_n - \varepsilon(y_n, a_k^0)] \left(\frac{\partial \varepsilon}{\partial a_j}\right)_{a_j = a_j^0}, \qquad [18]$$

results in

$$A \cdot \Delta a = U, \qquad \Delta a = A^{-1} \cdot U, \qquad a = a^0 + \Delta a. \qquad [19]$$

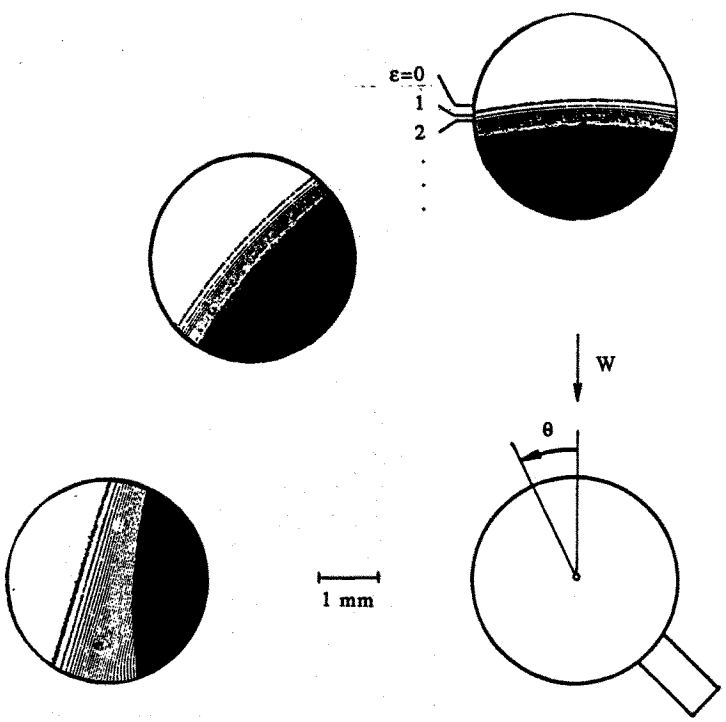

Figure 4. Interferogram of a heated sphere in ethanol.

By solving this matrix equation we obtain the coefficients of the polynomial for the refractive index field. If the dependence, dn/dT, of the refractive index n on the temperature, T is known, the heat transfer coefficient can then be calculated with the following equation:

$$h = \frac{-k\left(\frac{\partial T}{\partial y}\right)_w}{T_w - T_\infty}. \qquad [20]$$

Verification tests of the forced convection on a heated sphere were made to check the correction procedure mentioned above. It was found that better reconstruction can be achieved with the correction procedure and the optically obtained results agree with additional thermocouple measurements to $\pm 7\%$. From an uncertainty analysis based on the method proposed by Klein & McKlintock (1953), the uncertainty of the heat transfer coefficient h is estimated within $\pm 10\%$. An enlarged interferogram of the thermal boundary layer on a heated sphere is shown as an example in figure 4.

4. RESULTS AND EMPIRICAL CORRELATION

Figures 5 and 6 show interferograms of a condensing bubble at different Ja values. As can be seen, with low Ja the situation in the boundary layer varies considerably during bubble formation and bubble detachment and is quite different at the bubble top and the bubble root, as figure 5 demonstrates. In the first few milliseconds the bubble is growing slowly by vapor addition out of the nozzle and a quite stable laminar boundary layer can be observed around the bubble. At the instant when the detachment of the bubble starts, the boundary layer becomes considerably thinner at the upper surface of the bubble. The lower end of the bubble shows small oscillations, producing high turbulent vortices in the drift flow. With high Ja, which correspond to a much higher subcooling, the situation around the bubble is completely different, as figure 6 demonstrates. The phase interface becomes very unstable immediately due to local condensation effects and no laminar boundary layer can be observed around the bubble, which condenses completely within a very short period of approx. 10 ms. Under these conditions the inertia of the liquid governs the bubble collapse.

The holographic interferograms showed, at least at the top of the bubble, an effect of the relative velocity between the bubble and liquid on the heat transfer coefficient or the Nusselt number (Nu), respectively, similar to that of a solid sphere under cross flow conditions. Therefore, it was obvious to perform a trial to correlate the heat transfer by using the well-known equation

$$\mathrm{Nu} = C\,\mathrm{Re}^m\,\mathrm{Pr}^n. \qquad [21]$$

Using the bubble diameter at the moment of detachment as the characteristic length in the Nu and Re and by carefully averaging the measured data the correlation

$$\mathrm{Nu} = 0.6\,\mathrm{Re}^{0.6}\,\mathrm{Pr}^{0.5} \qquad [22]$$

was found for describing the mean heat transfer coefficient around the upper-half of the bubble, during the period when the bubble is still connected to the nozzle, i.e. before bubble detachment. The mean heat transfer coefficient was calculated from the local values taken along the bubble circumference at intervals of 10^0. Only these bubbles with their diameter not deviating from that at the moment of detachment, e.g. shortly before detachment, were taken into account. Examples can be given as shown in figure 7. In the calculation of Re, the relative velocity, i.e. the difference between the vertical velocity of the bubble center and that of the approach velocity of the liquid, was used. This equation is experimentally verified for Re values between 100 and 1000, Pr values between 6 and 20 and Ja values between 5 and 40. The equation is based on the assumption that the heat transport resistance is only on the liquid, which is certainly true for pure vapor not containing non-condensible gases. In contrast to the conditions around a solid sphere, the velocity at the phase interface is not zero and therefore the exponent with the Pr is higher than that for

solid spheres. The influence of the liquid Pr on the heat transfer situation is demonstrated in figure 7, where interferograms of different substances with approximately equal values of Re and Ja are compared. A comparison between experimental data measured by holographic interferometry and the predictions of [22] are shown in figure 8. The heat transfer at the surface of the bubble sticking at the nozzle but exposed to a slow cross flow is higher than that around a solid sphere, which can be explained by the smaller shear stress at the phase interface and by the movability of the bubble surface.

With rising bubble, i.e. after detachment, the heat transfer conditions become more complicated. With the holographic technique, boundary layers down to 0.05 mm could be investigated. In cases of still thinner boundary layers or with turbulent fluid dynamic conditions around the phase interface the mean heat transfer coefficient h_m was then evaluated from the temporal decrease in the bubble volume via an energy balance:

$$h_m = -\frac{\rho_G h_{LG} V_0}{\frac{1}{2} A_0 (T_s - T_\infty) t_k}, \qquad [23]$$

where V_0 and A_0 are the volume and surface area of the bubble at detachment and t_k is the time of condensation. This temporal decrease was measured with high-speed cinematography. Figure 9 shows as an example the temporal decrease in the bubble volume. Measurements of the temporal decrease in the bubble volume were carried out with the aid of a film analyzer. In the film analyzer, the bubble pictures were enlarged and projected onto a screen with scale. For simplicity, the bubble size was measured with only one coordinate pair, which was taken as a rectangle round the bubble. With the assumption that the depth of the bubble is the same as the width, the volume of an ellipsoid and also the radius of a sphere with the same volume can then be calculated as follows:

$$R = \sqrt[3]{b^2 h}, \qquad [24]$$

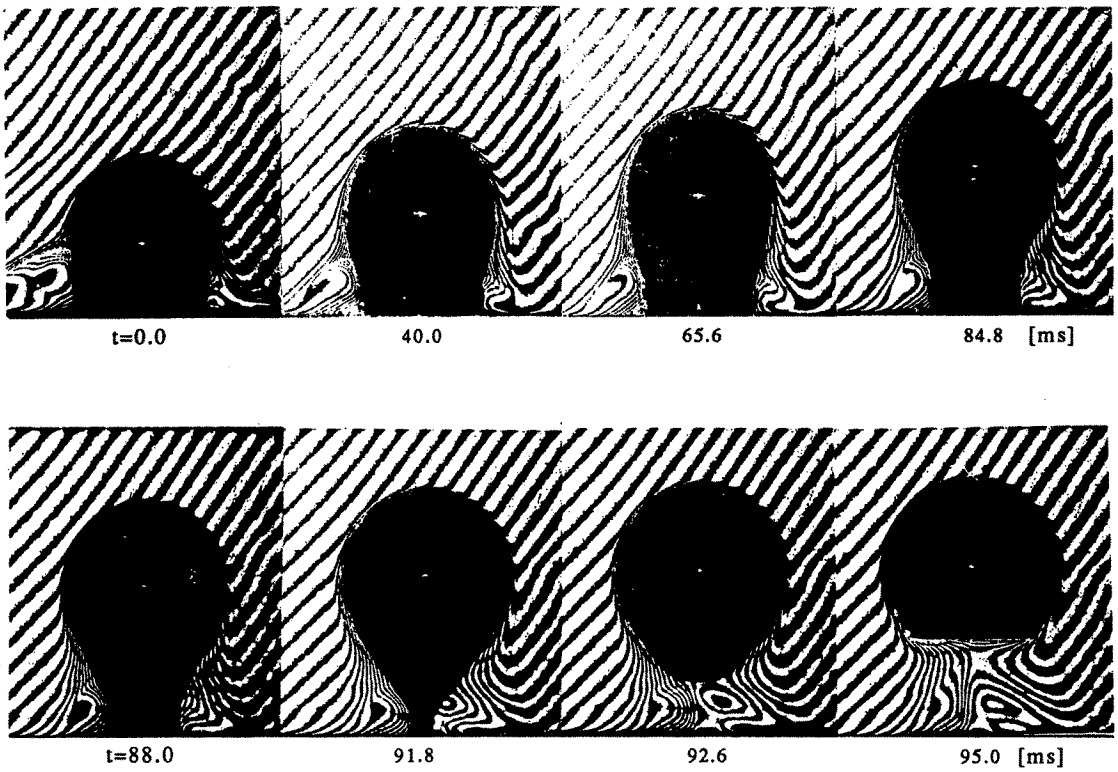

Figure 5. Interferograms of a condensing propanol bubble ($p = 2$ bar, $\Delta T = 7.6$ K, Ja = 7.1).

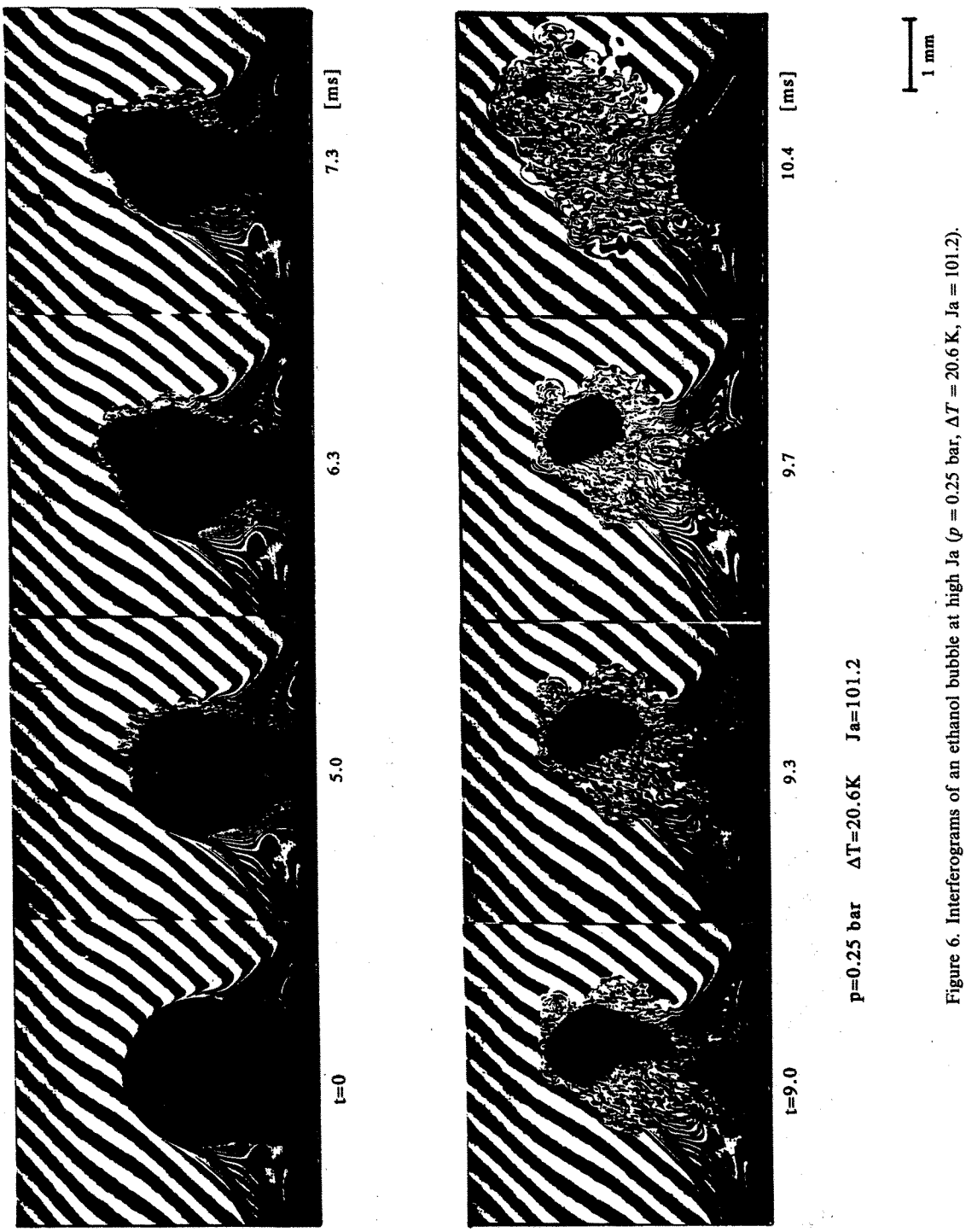

Figure 6. Interferograms of an ethanol bubble at high Ja ($p = 0.25$ bar, $\Delta T = 20.6$ K, Ja = 101.2).

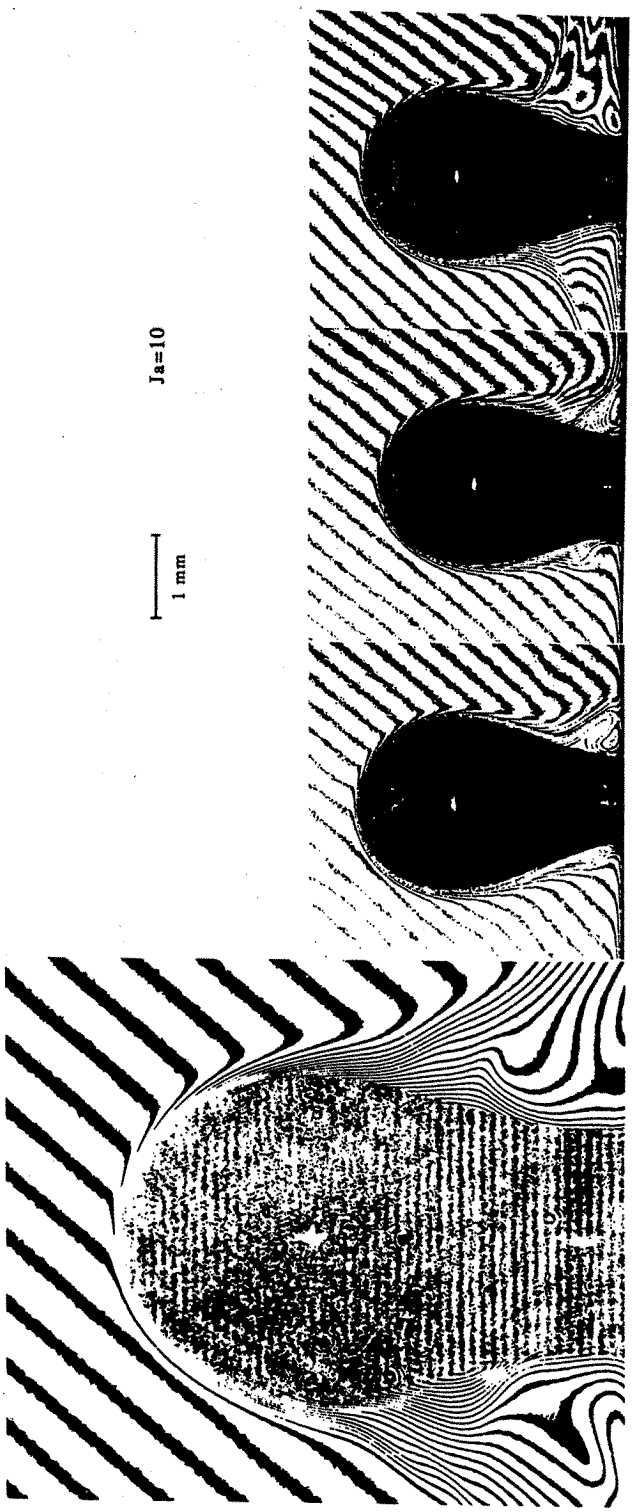

Figure 7. Comparison of boundary layer conditions with various Pr.

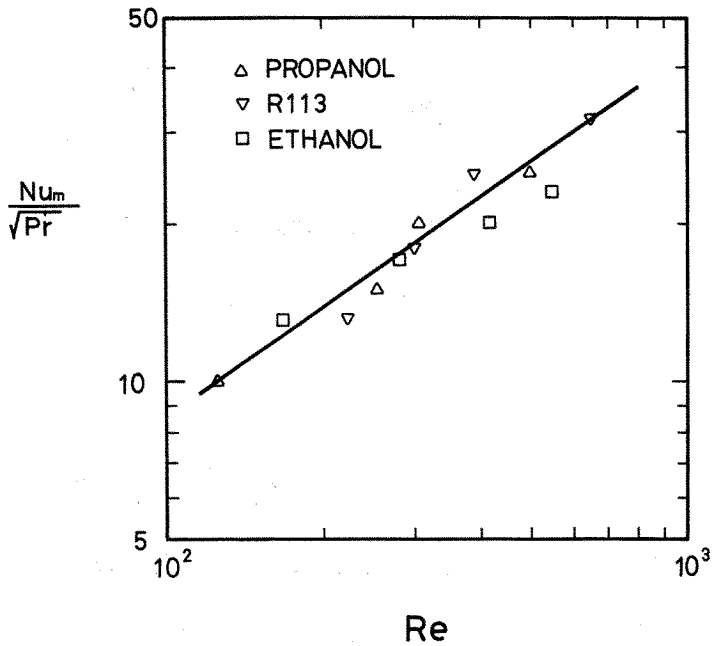

Figure 8. Comparison of experimental data from holographic interferometry with the empirical correlation.

where b is the width of the bubble and h is the height of the bubble. The time from frame to frame was registered through the timemarks (at intervals of 1 ms) which can be picked up on the edge of the high-speed film.

As expected, the high-speed cinematography showed that the bubbles reach a constant equilibrium velocity shortly after detaching from the nozzle. Therefore, an attempt was made to describe the heat transfer around rising bubbles with the same form of the correlation as that used for a sticking bubble. The question, however, is which characteristic length should be used in Nu and Re. Due to condensation the bubble diameter decreases continuously while the bubble is rising. Using the instantaneous bubble diameter would need a rather extensive and iterative procedure for calculating the heat transfer rate. In the literature, however, reliable equations can be found for correlating the bubble diameter at the moment of bubble detachment. Therefore (and with respect to a simpler procedure in practical use), the bubble diameter at the moment of detachment was used, which can be easily predicted by

$$d = \sqrt[3]{\frac{6\sigma d_n}{\Delta\rho g}}. \qquad [25]$$

With the least squares method the experimental results could be correlated in the simple form

$$\mathrm{Nu} = 0.185\,\mathrm{Re}^{0.7}\,\mathrm{Pr}^{0.5}, \qquad [26]$$

representing data up to $\mathrm{Re} = 10^4$. The low value 0.185 of the constant in [26] is because of the use of the detachment diameter as the characteristic length. As shown in figure 10, this correlation corresponds well with measured data of different substances. The correlation can be used up to $\mathrm{Ja} \sim 80$, as long as inertia effects do not play a dominant role.

The high-speed cinematography also gives information about the temporal decrease in the bubble diameter, which is closely related with the heat transfer at the phase interface. The duration of the bubble life can be expressed by the Fo in dimensionless form and using the experimental data the simple correlation

$$\mathrm{Fo} = 1.784\,\mathrm{Re}^{-0.7}\,\mathrm{Pr}^{-0.5}\,\mathrm{Ja}^{-1.0}, \qquad [27]$$

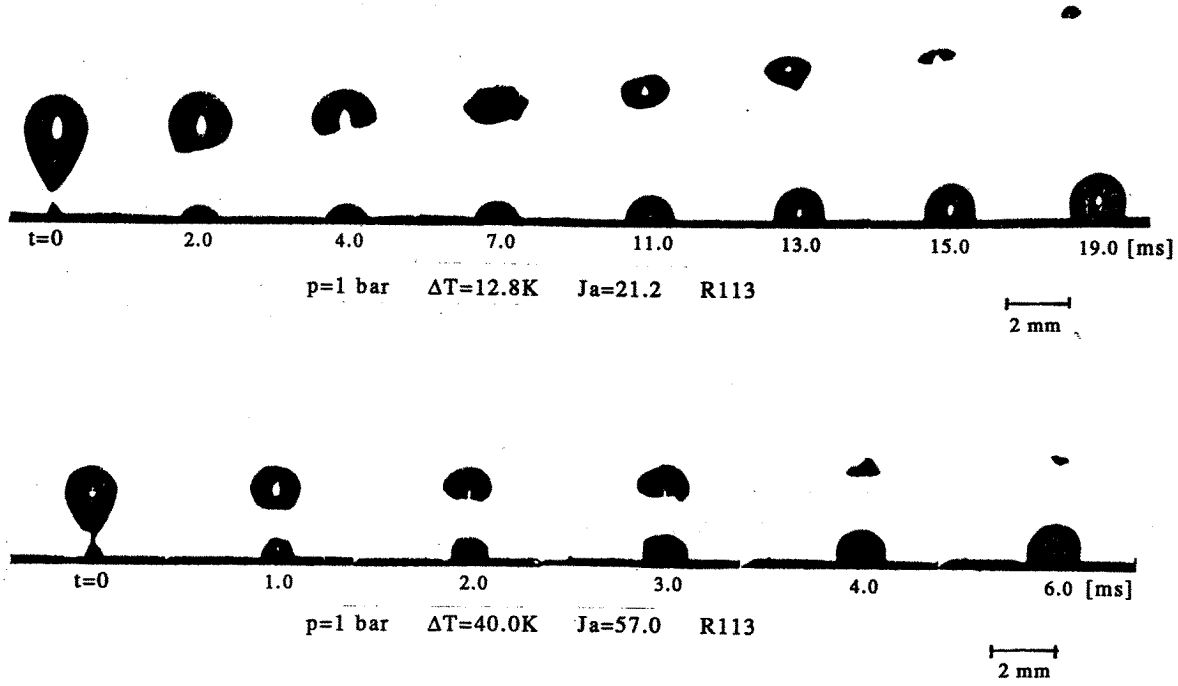

Figure 9. Temporal decrease in the bubble volume.

for predicting the total condensation period, was found. Up to Ja = 60 this equation corresponds well with the measured data, as figure 11 shows. When Ja > 80, the measured collapse Fo no longer depends on the Ja. This indicates also that above this Ja value the inertia forces play the dominant role.

The temporal decrease in the bubble diameter can be predicted using

$$\beta = (1 - 0.56\,\mathrm{Re}^{0.7}\,\mathrm{Pr}^{0.5}\,\mathrm{Ja}\,\mathrm{Fo})^{0.9}, \qquad [28]$$

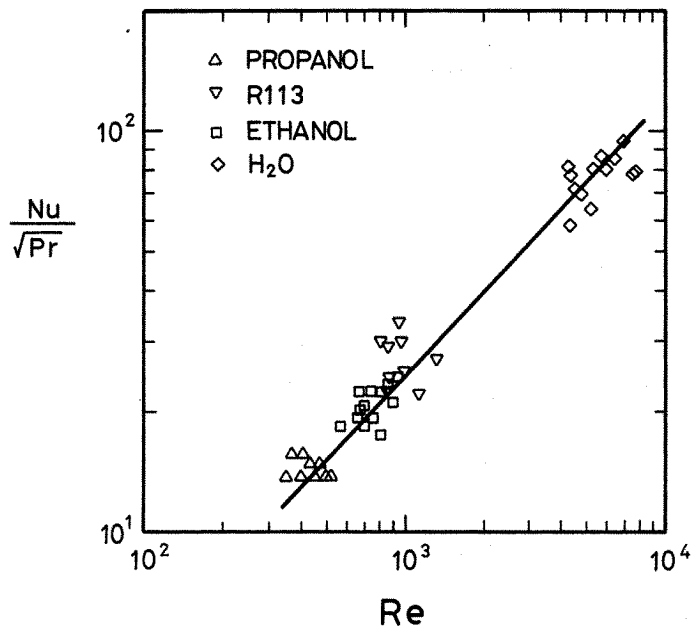

Figure 10. Mean Nu of rising bubbles, comparison with [26].

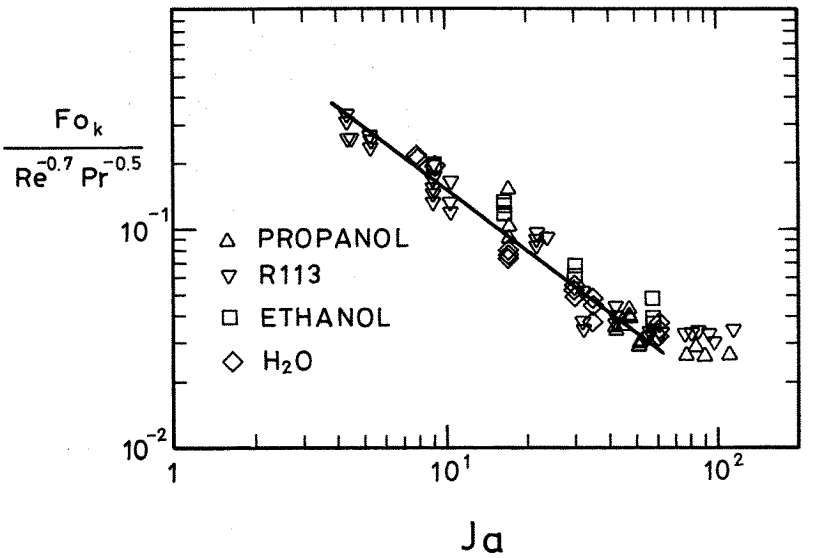

Figure 11. Condensation time, comparison of measured data with [27].

which was correlated from the data measured in this work, i.e. in the range $2 < Pr < 15$, $1 < Ja < 80$, $R_0 < 3$ mm. Comparison of the temporal decrease in the bubble diameter predicted from [28] and the equations listed in table 1 is shown in figure 12. In the equation from Floschuetz & Chao (1965), the translatory motion of the bubble is not considered, so that curve 1 looks qualitatively different from the others, particularly at the end stage of bubble collapse. Although curves 4–7 show a

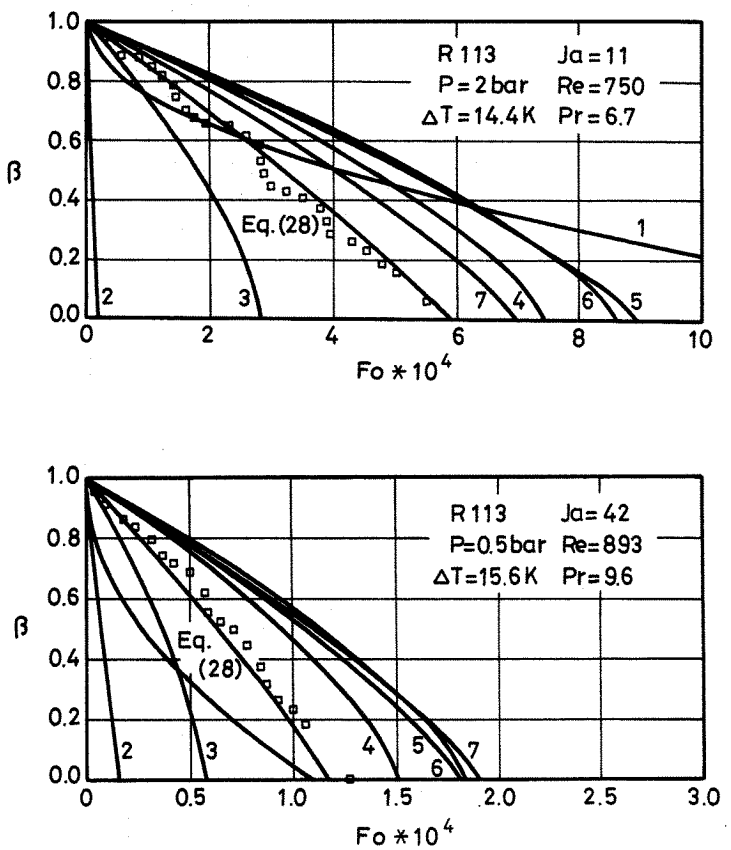

Figure 12. Comparison of the temporal decrease in the bubble diameter predicted by [28] and that listed in table 1.

Table 1. Equations predicting the temporal decrease in the condensing bubble diameter

Author(s)	Curve in figure 12	Equation	Remarks
Floschuetz & Chao (1965)	1	$\beta = \frac{R}{R_n} = 1 - \sqrt{\tau_H}$	$\tau_H = \frac{16}{\pi} \mathrm{Ja}^2 \mathrm{Fo}$
Voloshko & Vurgaft (1971)	2	$\beta = 1 - 6.776 \times 10^4 \mathrm{Fo}$	$40 < \mathrm{Ja} < 75$
Voloshko & Vurgaft *et al.* (1973)	3	$\beta = 1 - \left(\frac{6K}{\sqrt{2\pi}} \mathrm{Ja}\,\mathrm{Pe}^{1/2}\,\mathrm{Fo}\right)^{2/3}$	$K = 1.88$
Moalem & Sideman (1973)	4	$\beta = \left(1 - \frac{3}{\sqrt{3}} \mathrm{Ja}\,\mathrm{Pe}^{1/2}\,\mathrm{Fo}\right)^{5/7}$	$2 < R_0 < 4$ mm
	5	$\beta = \left(1 - \frac{5}{2}\frac{1}{\sqrt{\pi}} \mathrm{Ja}\,\mathrm{Pe}^{1/2}\,\mathrm{Fo}\right)^{4/5}$	$R_0 < 1$ mm
Akiyama (1973)	6	$\beta = (1 - 2.8C\,\mathrm{Pr}^{-0.27}\,\mathrm{Ja}\,\mathrm{Pe}^{0.6}\,\mathrm{Fo})^{5/7}$	$C = 0.37$
Dimic (1977)	7	$\beta = \left[1 - 5\frac{1}{\sqrt{\pi}}(3\zeta)^{-1/4}\,\mathrm{Ar}^{1/4}\,\mathrm{Pr}^{1/2}\,\mathrm{Ja}\,\mathrm{Fo}\right]^{4/5}$	$\mathrm{Re} > 3.1K_L^{0.25}$, $\zeta = 2.61$
	8	$\beta = \left[1 - 7\left(\frac{2.7}{\pi}\right)^{1/2} K_\sigma^{1/4}\,\mathrm{Ja}\,\mathrm{Fo}\right]^{407}$	$4.02K_L^{0.216} < \mathrm{Re} < 3.1K_L^{0.25}$

Peclet number $\mathrm{Pe} = (2R_0 w_0)/a_L$; Archimedes number $\mathrm{Ar} = g(2R_0)/\nu_L^2$.

similar trend to our own curve, the time of collapse predicted by [28] is apparently shorter. In the equation from Akiyama (1973), the heat transfer at the phase interface of the condensing bubbles is described as similar to that around a moving solid sphere. Equation [28] predicts a faster collapse than is given by the equation in Moalem & Sideman (1973) with a final collapse Fo about 25% lower than is given by their equation. The correlation developed by them is based on a potential flow type analysis. The equation from Voloshko & Vurgaft (1971) shows a very fast rate of bubble collapse. This may be attributed to the higher bubble frequency and larger bubble size in their experimental condition.

5. CONCLUSIONS

The measurements with holographic interferometry and high-speed cinematography show that the heat tansfer and volumetric decrease of pure vapor bubbles condensing in a subcooled liquid of the same substance can be reliably correlated using the dimensionless Ja, Re, Pr and Fo. The Ja value gives a clear indication of whether the heat transfer or the inertia is dominant in the condensing process. Up to Ja = 60 to 80 the condensation is purely controlled by the heat transfer at the phase interface. After a situation of mixed conditions (heat transfer and inertia), with Ja > 100, inertia forces then start to become the exclusive effect.

Acknowledgement—The authors wish to thank the Deutsche Forschungsgemeinschaft for financial support of this work.

REFERENCES

AKIYAMA, M. 1973 Bubble collapse in subcooled boiling. *Bull. JSME* **16**(93), 530–575.

DIMIC, M. 1977 Collapse of one-component vapour bubbles with translatory motion. *Int. J. Heat Mass Transfer* **20**, 1322–1325.

FLOSCHUETZ, L. W. & CHAO, B. T. 1965 On the mechanics of vapour bubble collapse. *J. Heat Transfer* **87**, 209–220.

HAMMITT, F. G. 1980 *Cavitation and Multiphase Flow Phenomena.* McGraw-Hill, New York.

HAMMITT, F. G. & KLING, C. L. 1972 A photographic study of spark induced cavitation bubble collapse. *J. Bas. Engng* **94**, 824–833.

HAUF, W. & GRIGULL, U. 1970 Optical methods in heat transfer. In *Advances in Heat Transfer*, Vol. 6, pp. 267–274. Academic Press, New York.

KLEIN, S. J. & MCCLINTOCK, F. A. 1953 Describing uncertainty in single sample experiments. **75,** 3–8.

MOALEM, D. & SIDEMAN, S. 1973 The effect of motion on bubble collapse. *Int. J. Heat Mass Transfer* **16,** 2321–2329.

NORDMAN, D. & MAYINGER, F. 1981 Temperature, Druck und Warmetransport in der Umgebung kondensierender Blasen. *VDI Forsch.* **605,** 3–36.

PLESSET, M. S. & PROSPERETTI, A. 1979 Bubble dynamics and canitation. *J. Appl. Mech.* **16,** 277–282.

RAYLEIGH, L. 1917 On the pressure developed in a liquid during the collapse of a spherical cavity. *Phil. Mag.* **34,** 94–98.

THEOFANOUS, T. G., BIASI, L., ISBIN, H. S. & FAUSKE, H. K. 1970 Non-equilibrium bubble collapse—a theoretical study. *Chem. Engng Prog. Symp. Ser.* **66**(102), 37–47.

VOLOSHKO, A. A. & VURGAFT, A. V. 1971 Study of condensation of single vapour bubbles in a layer of subcooled liquid. *Heat Transfer Sov. Res.* **3,** 2–7.

VOLOSHKO, A. A., VURGAFT, A. V. & AKSEL'ROD, L. S. 1973 Condensation of vapour bubbles in a liquid. Translated from *Theor. Osnovy Khim. Tekhnologii* **7,** 269–272.